Dynamic simulation analysis of molten salt reactor-coupled air-steam combined cycle power generation system

Jing-Lei Huang[1,2] , Guo-Bin Jia[1,*] , Li-Feng Han[1,*] , Wen-Qian Liu[1,2]

Affiliations:

[1]Shanghai Institute of Applied Physics, Chinese Academy of Sciences, Shanghai 201800, China

[2]University of Chinese Academy of Sciences, Beijing 100049, China

[*]Corresponding author. E-mail address: jiaguobin@sinap.ac.cn

[*]Corresponding author. E-mail address: hanlifeng@sinap.ac.cn

Abstract

A nonlinear dynamic simulation model based on coordinated control of speed and flow rate for the molten salt reactor and combined cycle systems is proposed here to ensure the coordination and stability between the molten salt reactor and power system. This model considers the impact of thermal properties of fluid variation on accuracy and has been validated with Simulink. This study reveals the capability of the control system to compensate for anomalous situations and maintain shaft stability in the event of perturbations occurring in high-temperature molten salt tank outlet parameters. Meanwhile, the control system's impact on the system's dynamic characteristics under molten salt disturbance is also analyzed. The results reveal that after the disturbance occurs, the controlled system benefits from the action of the control, and the overshoot and disturbance amplitude are positively correlated while the system power and frequency eventually return to the initial values. This simulation model provides a basis for utilizing molten salt reactors for power generation and maintaining grid stability.

Keywords: molten salt reactor; combined cycle; dynamic characteristic; control

1 Introduction

As a high energy density, clean, and low carbon energy, nuclear energy is an important means to ensure world energy security and promote energy conservation and emission reduction[1]. As one of the six candidate reactors of the fourth-generation advanced reactor, the molten salt reactor has become a research hotspot owing to its advantages of good neutron economy, inherent safety, online post-processing, less radioactive waste, sustainable development, anti-nuclear diffusion, and availability of thorium fuel[2], [3]. The molten salt reactor combined cycle power generation system has the advantages of small water demand, high energy utilization rate, and environmental friendliness. As the technology of molten salt reactors continues to mature and be applied, there is an increasing demand for stability in the power

generation of molten salt reactor generating systems. When the temperature and flow rate of the molten salt outlet change, significant variations in the system's parameters can affect its output power and, consequently, impact the stability of the power system.

The concept of a combined cycle involves the integration of multiple thermal cycles, specifically a front- and back-end cycle[4]. Typically, the Brayton cycle, primarily powered by gas turbines operating at high temperatures and utilizing high-grade heat, constitutes the front-end cycle. However, the Rankine cycle, which utilizes low-grade heat and operates in the low-temperature range, is dominated by steam turbines and forms the back-end cycle. By leveraging the high average heating temperature of the Brayton cycle and the low average cooling temperature of the Rankine cycle, the combined cycle can capitalize on the benefits of both cycles while addressing their incomplete energy utilization, enabling it to achieve high energy utilization efficiency. In addition, combined cycle technology exhibits a high level of maturity, which sets it apart from supercritical carbon dioxide cycles that encounter difficulties in sealing key components, system stability, and energy conversion mechanisms. Currently, the focus of combined cycle applications is primarily on three aspects. First, quickly starting up and providing load-balancing capabilities during periods of low demand can enhance flexibility when integrating large-scale renewable energy under "carbon neutrality" conditions. Second, the development of transition strategies from conventional coal-fired power generation to renewable energy-based electricity generation. Third, combining cycle technology to achieve higher thermal efficiencies compared to single-cycle gas turbine systems improves overall energy utilization efficiency[5].

Numerous scholars have conducted extensive research on the dynamic modeling of combined cycle systems, resulting in significant achievements in simulating load distribution and control systems of gas–steam combined cycles[6]–[9]. Zhang et al.[10] employed the Simulink simulation platform to establish a simulation model of the S109FA gas-steam combined cycle system, enabling them to obtain the operational and dynamic response characteristics of the S109FA combined cycle power plant. Zhang et al.[11] established a model of a gas turbine combined power generation system based on biomass gas and studied the influence of biomass gas flow rate and initial temperature on the efficiency of the combined power generation system. Ren et al.[12] combined blast furnace gas with the combined cycle system according to the working mechanism and structural parameters of the combined cycle, and deeply studied the dynamic simulation of the combined cycle system under the step disturbance of fuel composition, fuel bypass valve opening, and IGV opening. Fan et al.[13] proposed the utilization of molten salt energy storage in the combined cycle system. The release and storage of energy through molten salt in the peak and valley of power consumption can improve the system efficiency of the gas–steam combined cycle system and bring a good economy to the power plant. Sun et al.[14] built a natural gas combined cycle energy system and evaluated the economy and safety of distributed energy in the combined cycle system, which has a good guiding significance for the operation and control optimization of distributed energy systems.

Research on dynamic simulation of combined cycle power generation systems based on molten salt reactors started late in China, and there are a series of technical problems, such as immature operation optimization and control technology[15],[16]. Various technologies are related to molten salt energy storage, but critical technologies are still lacking. Simultaneously, the combined cycle system is a nonlinear, multivariable, strongly coupled controlled object, and conventional control strategies make it difficult to realize various indicators for complex multivariable systems. To fully address these issues and achieve stability in the molten salt reactor power generation, a simulation model must be established to accurately reflect the operational status of various system components in real time. This model should be able to reduce the impact of molten salt fluctuations on the system and provide support for system optimization. This paper combines molten salt reactors, open-air Brayton cycles, and steam Rankine cycles to establish an appropriate static and dynamic mathematical model. It utilizes Simulink to conduct interface and dynamic simulation experiments of the combined cycle power generation system.

2 Numerical model

2.1 System description

As presented in Fig. 1, in the overall system of the molten salt reactor with a combined cycle for power generation, the liquid fuel salt of the first loop enters the core. The fuel salt undergoes nuclear fission reactions and releases fission energy primarily in the form of heat. The fuel salt acts as a coolant and transports the heat out of the core. The heat is then transferred to the coolant salt of the second loop through a dual molten salt heat exchanger located between the two loops. Typically, the coolant salt in the second loop is FLiNaK molten salt. The first loop is isolated for safety purposes utilizing the second loop. This paper introduces a third loop utilizing nitrate salts to achieve safe load following for nuclear plants, where the heat is stored in a high-temperature molten salt tank[17]. When electricity is needed, the high-temperature molten salt is released from the tank, and the heat is transferred to compressed air through a heat exchanger in the fourth loop. The resulting high-temperature, high-pressure gas drives the turbine to generate electricity, converting the thermal energy into electrical energy. Simultaneously, the heat from the high-temperature exhaust gas produced by the gas turbine is recovered by a waste heat boiler, generating steam that enters a steam turbine generator for power generation. The study systematically analyzes the impact of three-loop molten salt regulation on the back-end power generation unit.

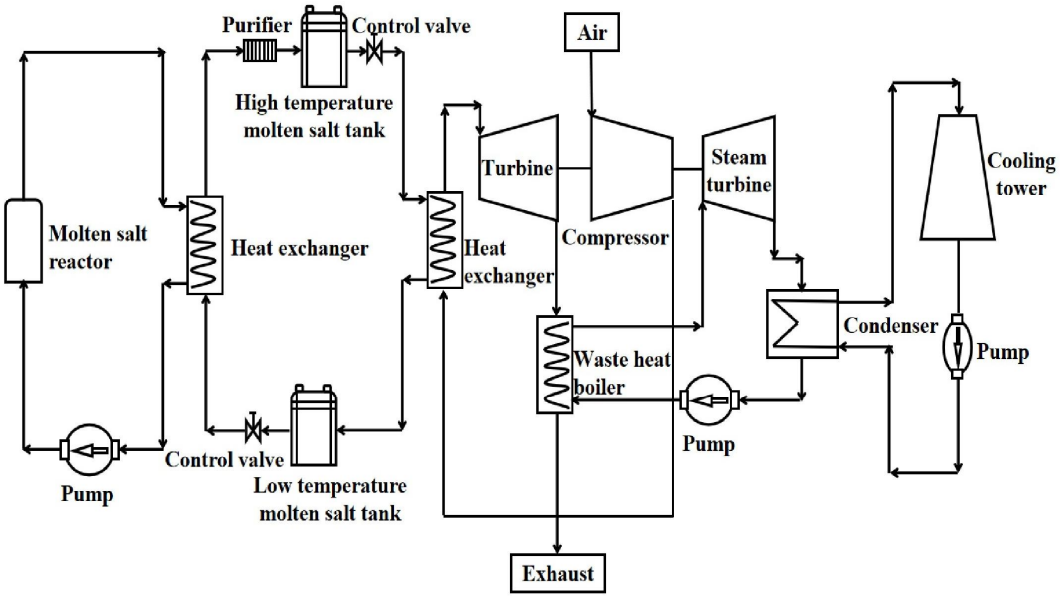

Fig. 1 Process of molten salt reactor combined cycle.

2.2 Compressor

The compressor module comprises characteristics such as temperature rise, flow rate, power consumption, and other modules, which can effectively reflect the operating dynamic characteristics of the compressor. The characteristic module describes the operating state of the compressor through the characteristic curve. The characteristic curve is drawn by an equivalent flow g_c, equivalent rotary speed n_s, pressure ratio π_c and efficiency $\eta_{iso,c}$, which is suitable for different inlet temperatures and pressure. The characteristic curve is represented as a two-dimensional table after obtaining a large amount of experimental data from the performance test of the compressor. The equivalent flow rate and compressor efficiency can be obtained on the characteristic curve by determining the compressor's pressure ratio and equivalent rotary speed. The pressure ratio and equivalent rotary speed of the compressor can be determined as follows[18]:

$$\pi_c = \frac{P_{c,out}}{P_{c,in}} \tag{1}$$

$$n_s = \frac{n_c}{\sqrt{T_{c,in}}} \tag{2}$$

where $P_{c,in}$ and $P_{c,out}$ are the compressor inlet pressure and outlet pressure, Pa; n_c is the actual speed of the compressor, rpm; $T_{c,in}$ is the actual inlet temperature of the compressor, K.

As the physical compressor of this paper has not yet been obtained, a coefficient fitting method can be utilized to obtain the compressor characteristic curve suitable for this paper[19]. The flow rate module of the compressor is defined as follows.

$$g_{c,in} = \frac{g_c \cdot P_{c,in}}{\sqrt{T_{c,in}}} \tag{3}$$

where $g_{c,in}$ is the actual flow of the compressor, kg/s.

A compressor's temperature rise and power consumption module represent its actual work capacity. The definition of the temperature rise module and power

consumption module of a compressor are as follows[20].

$$T_{c,out} = T_{c,in} + T_{c,in} \cdot |\pi_c^{\frac{k-1}{k}} - 1| \cdot \frac{1}{\eta_{iso,c}} \quad (4)$$

$$N_c = g_{c,in} \cdot C_{p,air} T_{c,in} \cdot |\pi_c^{\frac{k-1}{k}} - 1| \cdot \frac{1}{\eta_{iso,c}} \quad (5)$$

where $T_{c,out}$ is the compressor outlet temperature; K; k is the specific heat capacity ratio, k = 1.4; $C_{p,air}$ is the specific heat capacity of air at constant pressure, J/kg·K.

2.3 Molten salt-air heat exchanger

This study focused on the heat transfer process of a molten salt-air heat exchanger, which involved convective heat transfer on both the molten salt and air sides. In ideal conditions, based on the principle of energy conservation, the heat released by the high-temperature molten salt is equal to the heat absorbed by the air. The static heat transfer equation for the molten salt-air system can be described as follows[21].

$$q_{air} \cdot C_{p,air} \cdot (t_{air,out} - t_{air,in}) = KS\Delta T_m \quad (6)$$

$$q_{xcl} \cdot C_{p,xcl} \cdot (t_{xcl,in} - t_{xcl,out}) = KS\Delta T_m \quad (7)$$

$$\Delta T_m = \frac{(t_{xcl,in} - t_{xcl,out}) - (t_{air,out} - t_{air,in})}{ln(\frac{(t_{xcl,in} - t_{xcl,out})}{(t_{air,out} - t_{air,in})})} \quad (8)$$

where q_{air} is the air flow rate, kg/s; q_{xcl} is the molten salt flow rate, kg/s; $t_{air,in}$ is the air inlet temperature, K; $t_{air,out}$ is the air outlet temperature, K; $t_{xcl,in}$ is the molten salt inlet temperature, K; $t_{xcl,out}$ is the molten salt outlet temperature, K; $C_{p,xcl}$ is the specific heat capacity of molten salt at constant pressure, J/kg·K; k is the heat transfer coefficient, W/($m^2 \cdot K$); S is the total heat transfer area, m^2; ΔT_m is the effective average temperature difference, K.

It is difficult to determine the heat transfer coefficient under variable conditions, hence, the heat transfer coefficient within the error can only be obtained by analyzing the heat transfer principle. Regarding ignoring thermal radiation, heat conduction and convective heat transfer are the main heat transfer in this process. The heat transfer coefficient can be defined as follows.

$$\frac{1}{K} = \frac{1}{\alpha_o} + \frac{1}{\alpha_i}(\frac{A_o}{A_i}) + r_o + r_i(\frac{A_o}{A_i}) + \frac{\delta A_o}{\lambda_w A_m} \quad (9)$$

where α_o is the convective heat transfer coefficient of the fluid outside the tube, W/($m^2 \cdot K$); α_i is the convective heat transfer coefficient of the fluid in the tube, W/($m^2 \cdot K$); r_o and r_i are the fluid fouling resistance outside the tube and inside the tube ($m^2 \cdot K$)/W; A_o and A_i are the outer surface and inner surface heat transfer area of the heat exchange tube, m^2; A_m is the average heat transfer area inside and outside the heat exchanger tube, m^2; δ is the thickness of the heat exchange tube wall, m; λ_w is the thermal conductivity of the tube wall material, W/($m^2 \cdot K$).

2.4 Turbine

Like the compressor module, the turbine module can be described by its characteristic curve to represent its operating characteristics. The turbine module comprises a characteristic module, a temperature drop module, and a power generation module. In the characteristic module, the characteristic curve of the turbine can also be obtained with the coefficient fitting method. The pressure ratio and flow rate of the turbine are determined as follows[22].

$$\pi_t = \frac{P_{t,in}}{P_{t,out}} \tag{10}$$

$$g_{t,in} = \frac{g_t \cdot P_{t,in}}{\sqrt{T_{t,in}}} \tag{11}$$

where π_t is the pressure ratio of the turbine; g_t is the equivalent flow rate; $\eta_{ios,t}$ is the turbine efficiency; $P_{t,in}$ is the turbine inlet pressure, Pa; $P_{t,out}$ is the turbine outlet pressure, Pa; $T_{t,in}$ is the turbine inlet temperature, K.

The outlet temperature and turbine work can be expressed as follows[23].

$$T_{t,out} = T_{t,in} - T_{t,in} \cdot |1 - \pi_t^{\frac{k-1}{k}}| \cdot \eta_{iso,t} \tag{12}$$

$$N_t = g_{t,in} \cdot C_{p,air} T_{t,in} \cdot |1 - \pi_t^{\frac{k-1}{k}}| \cdot \eta_{iso,t} \tag{13}$$

where $T_{t,out}$ is the turbine outlet temperature, K; N_t is the turbine output power, W.

2.5 Rotor

Any set point of the engine is defined by the amount of power demanded by the grid and the frequency at which the power is to be generated. Thus, the power turbine must rotate constantly at 8000 rpm–50 Hz for direct coupling between the engine and generator or at another speed if a gearbox is present. Considering that the compressor and the turbine are coaxial in the system, assuming the same speed, the differential equation of the rotor module given by reference can be defined as[24]

$$\frac{dn}{dt} = \frac{900}{I \cdot \pi^2 \cdot n}(N_t - N_c) \tag{14}$$

where I is the moment of inertia of the rotor, kg·m^2; n is the rotary speed, rpm.

2.6 Waste heat boiler

The construction of the waste heat boiler module is like that of the molten salt air heat exchange module. The heat transfer process of the boiler involves the convective heat transfer on the water and air sides. According to the energy conservation equation, it can be concluded that the heat release of air is equal to the heat absorption of the waterside under ideal conditions, which can be expressed as follows[25].

$$q_{air} \cdot (h_{air,in} - h_{air,out}) = q_w \cdot (h_{w,out} - h_{w,in}) \tag{15}$$

where $h_{air,in}$ and $h_{air,out}$ are the enthalpy of inlet and outlet air of the waste heat boiler, J/kg; $h_{w,in}$ and $h_{w,out}$ are the enthalpy of inlet and outlet water of the waste heat boiler, J/kg; q_w is the water flow, kg/s.

2.7 Steam turbine

In the combined cycle, the steam turbine has no regulating stage; only the working stage is set, and the working medium is in a subcritical state during the entire working process. The calculation equations of the flow module and the work module

of the steam turbine are defined as follows[26]:

$$\frac{D}{D_0} = \sqrt{\frac{P_1^2 - P_2^2}{P_{10}^2 - P_{20}^2}} \sqrt{\frac{T_{10}}{T_1}} \quad (16)$$

$$P_e = D(h_1 - h_2) \quad (17)$$

where D is the main steam flow rate of the steam turbine, kg/s; P_1 and P_2 are the pressure of the inlet and outlet steam of the steam turbine, Pa; T_1 is the temperature of the inlet steam of the steam turbine, K; the subscript 0 represents the known standard working condition parameters; h_1 and h_2 are the enthalpy values of the steam at the inlet and outlet of the steam turbine.

2.8 Control logic

The control module is composed of a rotary speed control system, which guarantees stable and safe operation of the system. If the actual speed does not match the reference speed, the control system will output an appropriate signal to adjust the size of the molten salt flow rate and subsequently regulate the entire system. Fig. 2 presents the flowchart of the rotary speed control structure. The definition of rotary speed PID control algorithm is as follows[27]:

$$e_n = n_r - n_c \quad (18)$$

$$\Delta U_p = K_p(e_n - e_{n-1}) \quad (19)$$

$$\Delta U_i = K_i e_n \quad (20)$$

$$\Delta \mathrm{U_d} = \mathrm{K_d}(\mathrm{e_n} - 2\mathrm{e_{n-1}} + 2\mathrm{e_{n-2}}) \quad (21)$$

$$\Delta U = \Delta U_p + \Delta U_i + \Delta U_d \quad (22)$$

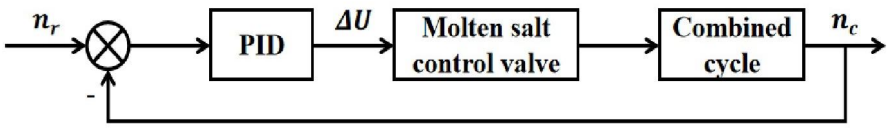

Fig. 2 Flowchart of rotary speed control structure.

where n_r is the current cycle speed reference, rpm; e_n is the deviation between the current cycle target speed and the actual speed, rpm; e_{n-1} is the deviation between the target speed and the actual speed in the previous cycle, rpm; e_{n-2} is the deviation between the target speed and the actual speed of the previous two cycles, rpm; K_p is the proportional coefficient; K_i is the coefficient of the integral term; K_d is the differential coefficient; ΔU_p is the proportional feedback; ΔU_i is the integral feedback; ΔU_d is the differential feedback; ΔU is the amount of feedback.

3. Establishment and verification of numerical model

3.1 Establishment of numerical model

Matlab-Simulink is a modeling platform supporting linear, nonlinear, continuous, and discrete-time systems, which can realize modeling, simulation, and analysis of dynamic systems[28]. Simulink can represent models in the form of block diagrams and can add existing models to a composite or user-developed module to a model. Simulink allows modification of the module parameters, and Matlab analyzes the

simulation results scientifically. The molten salt reactor combined cycle system model can be obtained by connecting each module on the Simulink. As presented in Fig. 3, the system comprises the compressor, molten salt tank, heat exchanger, turbine, rotor, waste heat boiler, and steam turbine.

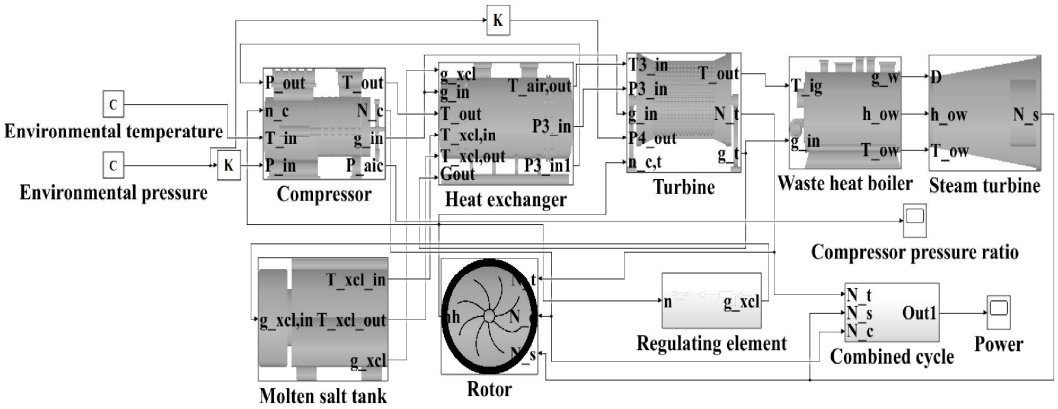

Fig. 3 Model of molten salt reactor combined cycle system.

As illustrated in Fig. 4, the output parameters of the compressor can be obtained by compressor inlet temperature $T_{c,in}$, inlet pressure $P_{c,in}$, actual speed n_c and outlet pressure $P_{c,out}$. The output parameters of the compressor are pressure ratio π_c, actual flow $g_{c,in}$, outlet temperature $T_{c,out}$, compressor efficiency $\eta_{iso,c}$ and power consumption N_c. The molten salt flow rate g_{xcl}, molten salt inlet temperature $t_{xcl,in}$, molten salt outlet temperature $t_{xcl,out}$ and compressor output parameters of the molten salt reactor are input into the molten salt air heat exchanger to obtain the flow rate of the turbine $g_{t,in}$, air temperature $t_{air,out}$, pressure $P_{t,in}$ and $P_{t,out}$ after heat transfer. The high-temperature air parameters are input into the turbine to obtain the turbine outlet exhaust temperature $T_{t,out}$, turbine flow rate $g_{t,out}$ and turbine power N_t. The enthalpy $h_{w,out}$ and flow rate of outlet water vapor g_w can be obtained by inputting the turbine outlet exhaust parameters into the waste heat boiler. The parameters of the outlet steam are input into the steam turbine to obtain the power of the steam turbine N_s. The n_c can be adjusted to realize the dynamic balance of the system by N_c, N_t and N_s.

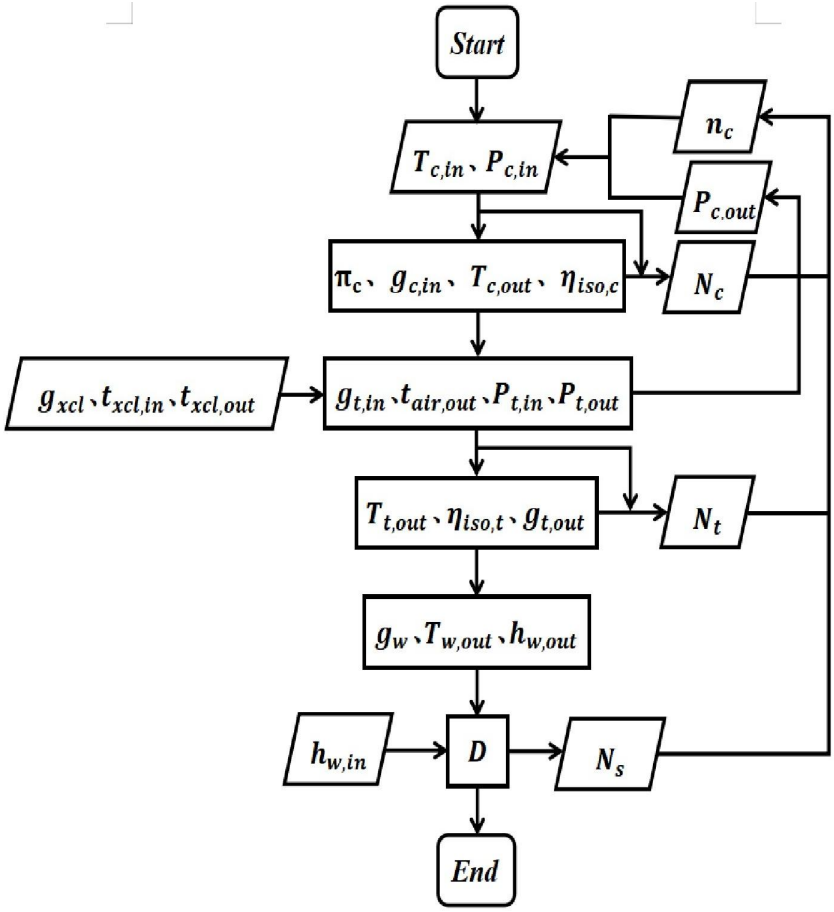

Fig. 4 Process of parameter calculation.

3.2 Verification of numerical model

The accuracy of the molten salt reactor combined cycle system model established here was ensured by validating the system simulation results. Comparing the performance of the simulated and actual systems is an appropriate method for verifying the simulation's accuracy. Here, the reliability of the simulated system was validated with the parameters of the S109FA combined cycle[10]. Table 1 presents the basic parameters of the S109FA combined cycle. Table 2 presents a comparison of the design value, calculation value, and simulation value of the S109FA combined cycle.

Table 1 Basic parameters of S109FA combined cycle.

System parameters	Design value
Environmental pressure/kPa	101.35
Environmental temperature/K	288
Inlet pressure loss coefficient	0.02
Power of gas turbine/MW	255.6
Power of steam turbine/MW	130
Net output power/MW	395.52
Inlet temperature of gas turbine /K	1600
Outlet temperature of gas turbine/K	877.7
Fuel flow rate/(kg·s^{-1})	14.1
Temperature of steam /K	838.6

Table 2 Comparison of design value, calculation value and simulation value of

S109FA combined cycle.

System parameters	Design value	Calculation value	error(%)	simulation value	error(%)
Inlet temperature of gas turbine/K	1600	1593	0.438	1591	0.563
Outlet temperature of gas turbine/K	877.7	876.7	0.114	874.9	0.319
Temperature of steam/K	838.6	837.6	0.119	838	0.072
Power of gas turbine/MW	255.6	256	-0.156	254.9	0.274
Power of steam turbine/MW	130	129.7	0.230	129.1	0.692
Net output power/MW	395.52	393.8	0.435	392.5	0.764

Table 2 presents the discrepancies between the simulated and the design values, and the calculated values of the S109FA combined cycle. The main reason for the error is the pressure loss caused by the flow of the working medium in the pipeline during the establishment of the numerical model. The dynamic simulation model of the combined cycle system established within a reasonable error has high accuracy and effectiveness.

4 Results and discussion

The intermediate loop of molten salt is primarily utilized for safety considerations. Because the first loop contains liquid fuel salt with radioactive substances, the second loop serves as a barrier to prevent the core from melting in case of a leak in the first loop. In addition, the system incorporates a molten salt energy storage loop, which enables the system to meet the load demand of the electrical grid and reduces the risk of the core losing its ultimate cold trap[29]. The molten salt reactor combined cycle power generation system utilizes the molten salt reactor as the energy supply end and the power generation system as the output end. The impact of disturbances in high-temperature molten salt tank outlet temperature and flow rate on plant operation was studied without considering the dynamic characteristics associated with startup and shutdown processes. Table 3 presents the basic operating parameters of the molten salt reactor combined cycle[30].

Table 3 Basic parameters of molten salt reactor combined cycle.

System parameters	Design value
Environmental pressure/kPa	101.3
Environmental temperature/K	293
Inlet pressure loss coefficient	0.01
Net output power/MW	3.549
Inlet temperature of gas turbine/K	923
Outlet temperature of gas turbine/K	602
Flow rate of molten salt/(kg·s^{-1})	43.69

4.1 Influence of high-temperature molten salt tank outlet temperature

This paper presents a simulation of a disturbance in the outlet temperature of a molten salt tank, potentially caused by poor circulation. Fig. 5 presents the introduction of various perturbations to the temperature at the outlet of the high-temperature molten salt tank at 200 s after reaching steady-state conditions. At

this point, the temperature commenced a simultaneous descent of 5 K and 10 K, with rates of -0.2 K/s and -0.4 K/s, respectively, from its initial value of 973 K. The temperature also exhibited concurrent increments of 5 K and 10 K, with corresponding rates of increase of 0.2 K/s and 0.4 K/s. These variations persisted for 25 s.

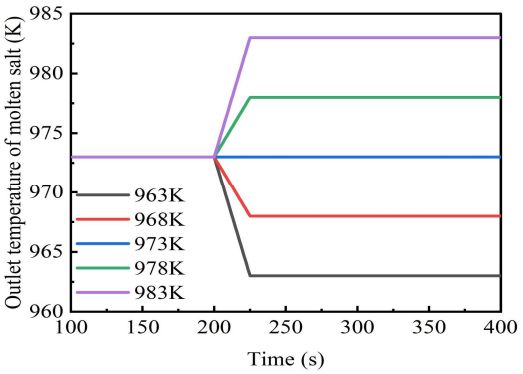

Fig. 5 Variations in outlet temperature of high-temperature molten salt tank.

The decrease in the outlet temperature of the molten salt from the high-temperature molten salt tank results in a reduction in the temperature of the molten salt entering the heat exchanger, thereby reducing the heat transfer between the molten salt and air. As presented in Fig. 6(a), this leads to a decrease in the inlet temperature of the turbine, resulting in a decrease in its rotational speed. As presented in Fig. 6(b), when the control component detects a rotational speed below the reference value, the speed controller outputs a signal to increase the flow rate of the molten salt. However, an increase in the outlet temperature of the molten salt from the high-temperature molten salt tank results in a rise in the temperature of the molten salt entering the heat exchanger, thereby increasing the heat transfer between the molten salt and air. This leads to an increase in the inlet temperature of the turbine, increasing its rotational speed. When the control component detects a rotational speed above the reference value, the speed controller outputs a signal to decrease the flow rate of the molten salt. With the help of the control system, the system ultimately returns to a stable state.

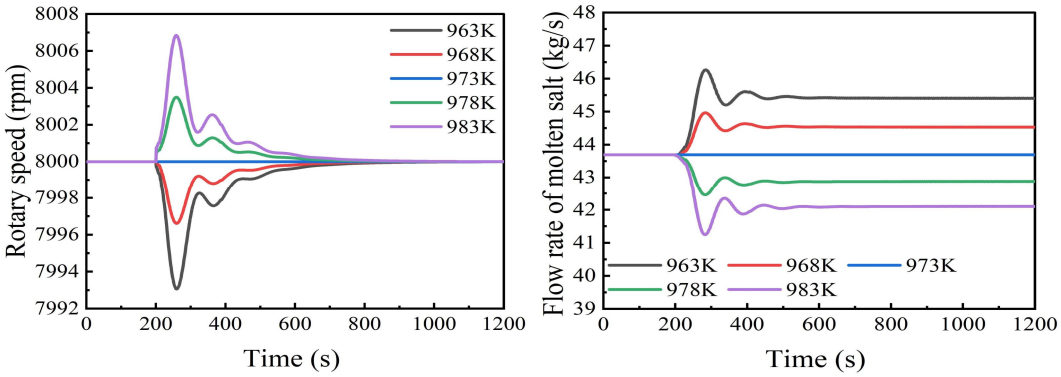

(a) Rotary speed (b) Flow rate of molten salt

Fig. 6 Variations in rotary speed and molten salt flow rate with changing outlet temperature.

Fig. 7 presents the power changes of the controlled and uncontrolled systems

when the molten salt outlet temperature decreases by 5 K and 10 K, respectively. In Fig. 7(a), the controlled system's output power deviation from its rated value is lower than 1.28% and 2.52%, respectively, under the regulation of the control system. In contrast, the uncontrolled system's output power deviation from its rated value is above 1.80% and 3.62%, respectively. Fig. 7(b) demonstrates that the control system compensates for decreased molten salt outlet temperature, ensuring the frequency deviation from its rated value is lower than 0.09%. In contrast, uncontrolled power systems cannot maintain shaft stability owing to a lack of regulation, resulting in frequencies falling below the lower limit of the grid frequency.

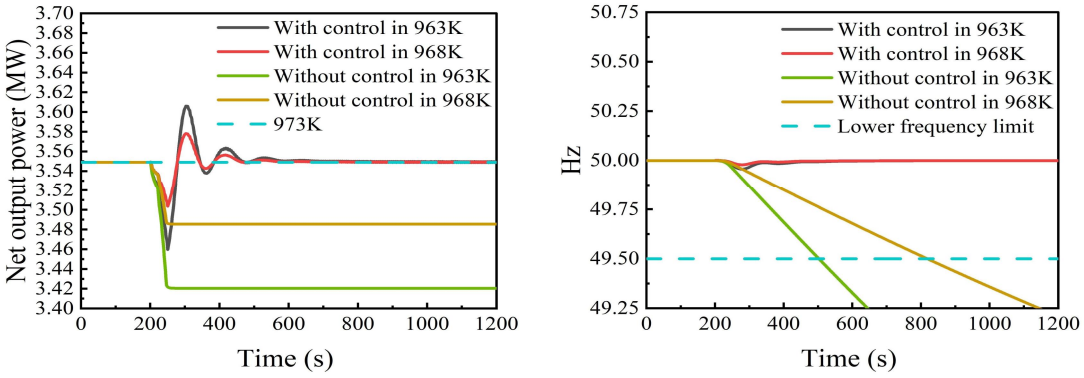

(a) Comparison of net output power (b) Comparison of grid frequency

Fig. 7 Effects of decreasing high-temperature molten salt tank outlet temperature by 5 K and 10 K on net output power and grid frequency variation.

Fig. 8 demonstrates the power changes of the controlled and uncontrolled systems when the molten salt outlet temperature increases by 5 K and 10 K, respectively. In Fig. 8(a), under the control system's regulation, the output power deviation from its rated value is lower than 1.19% and 2.43%, respectively. However, the uncontrolled system's output power deviation from its rated value is higher than 1.79% and 3.55%, respectively. Fig. 8(b) indicates that the control system can compensate for the molten salt outlet temperature increase, ensuring that the frequency deviation from its rated value is lower than 0.08%. Conversely, the uncontrolled system's frequency deviation exceeds the grid frequency upper limit.

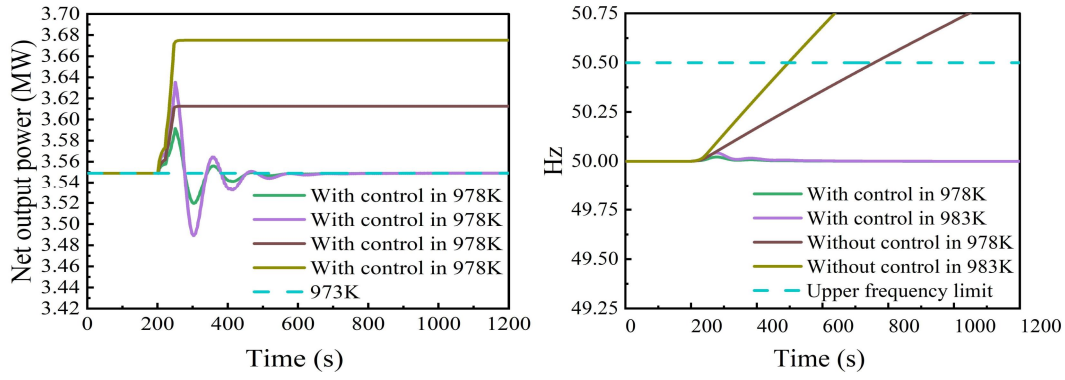

(a) Comparison of net output power (b) Comparison of grid frequency

Fig. 8 Effects of increasing high-temperature molten salt tank outlet temperature by 5 K and 10 K

on net output power and grid frequency variation.

4.2 Influence of high-temperature molten salt tank outlet flow rate

Here, we simulated the molten salt outlet flow disturbance scenario, which the molten salt level fluctuation inside the tank may cause. Fig. 9 presents the introduction of various perturbations to the flow rate at the outlet of the high-temperature molten salt tank at 200 s after reaching steady-state conditions. At this point, the flow rate commenced a simultaneous descent of 5% and 10%, with rates of -1 %/s and -2 %/s, respectively, from its initial value of 43.69 kg/s. The flow rate also exhibited concurrent increments of 5% and 10%, with corresponding rates of increase of 1%/s and 2%/s. These variations persisted for 5 s.

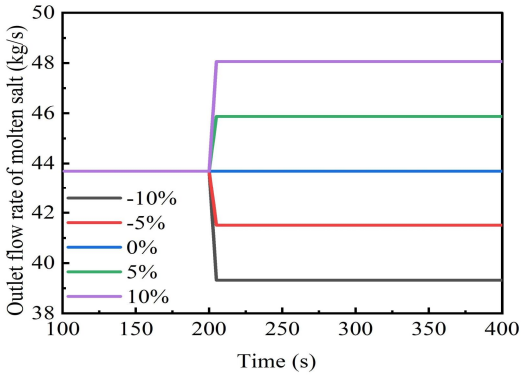

Fig. 9 Variations in outlet flow rate of high-temperature molten salt tank.

A reduction in the molten salt flow rate at the outlet of the high-temperature salt tank will decrease the molten salt's flow rate entering the heat exchanger. As illustrated in Fig. 10(a), with a decrease in heat transfer between the molten salt and air, the inlet temperature of the turbine decreases, resulting in a reduction of its rotational speed. As illustrated in Fig. 10(b), the control component monitored the speed, and when it fell below the reference value, the speed controller output a signal to increase the molten salt flow rate. Conversely, when the speed exceeds the reference value, the speed controller outputs a signal to decrease the molten salt flow rate. Through the adjustment of the control system, the turbine eventually returned to a stable state.

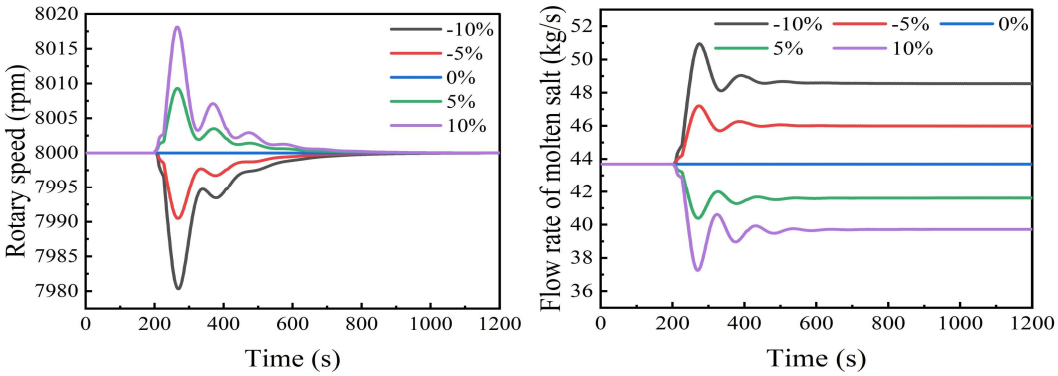

(a) Rotary speed (b) Flow rate of molten salt

Fig. 10 Variations in rotary speed and molten salt flow rate with changing outlet flow rate.

Fig. 11 presents the power changes of the controlled and uncontrolled systems

with 5% and 10% reductions in molten salt outlet flow rates. Fig. 11(a) illustrates that the controlled system maintained an output power deviation from its rated value of less than 4.06% and 8.2%, respectively, under the adjustment of the control system. In contrast, the uncontrolled system had an output power deviation above 4.82% and 9.80%, respectively. As presented in Fig. 11(b), the control system compensated for the decrease in the molten salt outlet flow rate, resulting in the frequency deviation from its rated value of less than 0.25%. However, the frequency of the uncontrolled system deviated from its rated value and ultimately exceeded the lower limit of the grid frequency.

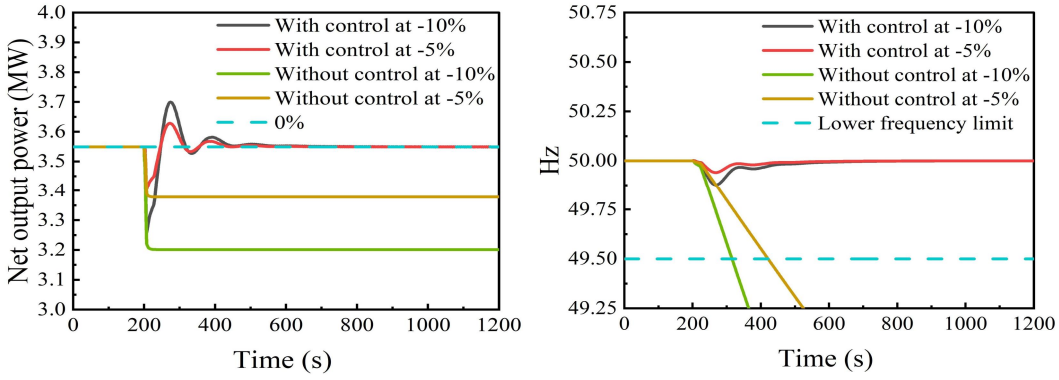

(a) Comparison of net output power (b) Comparison of grid frequency

Fig. 11 Effects of decreasing high-temperature molten salt tank outlet flow rate by 5% and 10% on net output power and grid frequency variation.

Fig. 12 presents the power changes of the controlled and uncontrolled systems with 5% and 10% increases in molten salt outlet flow rate. Fig. 12(a) illustrates that the controlled system maintained an output power deviation from its rated value of less than 3.82% and 7.56%, respectively, under the adjustment of the control system. In contrast, the uncontrolled system had an output power deviation above 4.68% and 9.20%, respectively. As illustrated in Fig. 12(b), the control system compensated for the increase in the molten salt outlet flow rate, resulting in the frequency deviation from its rated value of less than 0.22%. However, the frequency of the uncontrolled system deviated from its rated value and ultimately exceeded the upper limit of the grid frequency.

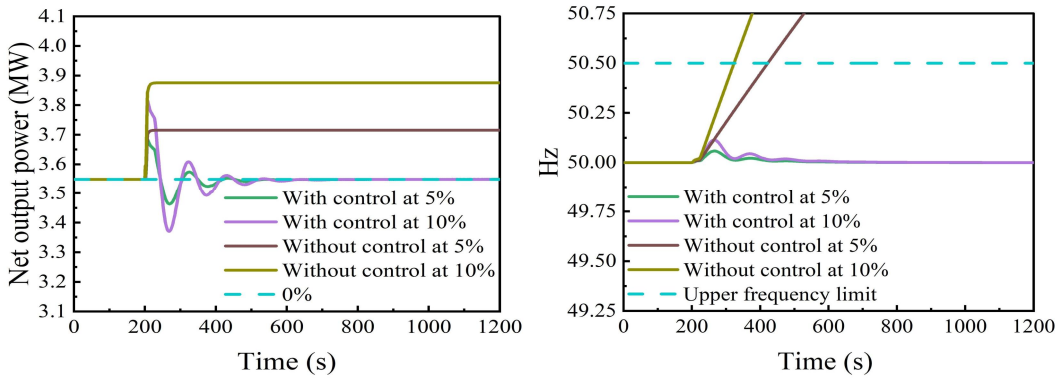

(a) Comparison of net output power (b) Comparison of grid frequency

Fig. 12 Effects of increasing high-temperature molten salt tank outlet flow rate by 5% and 10% on

net output power and grid frequency variation.

The simulation results of the power system indicate that the fluctuation of the high-temperature molten salt tank outlet parameters significantly impacts the system's operating parameters. First, introducing a control system can minimize the impact of different disturbances and maintain its output frequency in line with the grid. Second, under the control system's influence, the output power and frequency change gradually reduced and stabilized at the initial values. In contrast, the uncontrolled system had larger output power and frequency deviations, eventually deviating from the initial values.

5 Conclusion

This study established a dynamic simulation model of the molten salt reactor combined cycle system based on rotary-flow rate control. The model can be adjusted effectively when there are disturbances in the system. This significantly prevents rapid changes in the working fluid parameters from affecting system performance and ensures stable grid connection. The research findings are summarized as follows:

(1) A simulation model of the molten salt reactor combined cycle system was established, and the model's accuracy was validated on the Simulink platform with parameters of the S109FA combined cycle.

(2) A combined cycle system with a rotary-flow rate control based on a molten salt reactor has been established. Under the different perturbations of parameters at the outlet of the high-temperature molten salt tank, the system relies on its control to mitigate various disturbances and ensure that the output frequency of the system remains synchronized with that of the electric grid.

(3) A comparison was made between controlled and non-controlled systems in response to variations in outlet parameters of a high-temperature molten salt tank. Results revealed that after a certain period, the controlled system's output power and grid frequency returned to their initial values. However, those of the non-controlled system deviated from the initial values. Furthermore, the disturbance caused by variations in the outlet parameters of the high-temperature molten salt tank resulted in a larger overshoot in the controlled system as the magnitude of the perturbation increased.

Author contributions: All authors contributed to the study conception and design. Material preparation, data collection and analysis were performed by Jing-Lei Huang, Guo-Bin Jia, Li-Feng Han and Wen-Qian Liu. The first draft of the manuscript was written by Jing-Lei Huang and all authors commented on previous versions of the manuscript. All authors read and approved the final manuscript.

Data Availability Statement: The data that support the findings of this study are openly available in Science Data Bank at https://cstr.cn/31253.11.sciencedb.j00186.00118 and https://doi.org/10.57760/sciencedb.j00186.00118.

References

[1] X.Z. Cai, Z.M. Dai, H.J. Xu, Thorium molten salt reactor nuclear energy s ystem. Physics **45**, 578-590 (2016). https://doi.org/10.7693/wl20160904

[2] M.S. Cheng, Z.M. Dai, Development of a three dimension multi-physics co de for molten salt fast reactor. Nucl. Sci. Tech. **25**, 010601 (2014). https://doi.

org/10.13538/j.1001-8042/nst.25.010601
[3] G.C. Li, Y. Zou, C.G Yu et al., Influences of 7Li enrichment on Th–U fuel breeding for an Improved Molten Salt Fast Reactor(IMSFR). Nucl. Sci. Tech. **28**, 97 (2017). https://doi.org/10.1007/s41365-017-0250-7
[4] Z. Guo, Design of automatic control system for gas turbine. (Machinery Press, Beijing 1986)
[5] X.S. Zhang, T. Ding, M. Qu et al., Review on system Commitment Modeling Considering Combined-cycle Gas Turbine. Proceedings of the CSEE. **43**, 969-987 (2023). https://doi.org/10.13334/j.0258-8013.pcsee.212457
[6] B.S. Wang, N. Cui, C.S. Zhang et al., Dynamic Simulation Model for Gas-steam Combined Cycle Thermodynamic System. J. Syst. Simul. **20**, 3107-3113 (2008).
[7] B. Sun, Y.W. Liu, X. Chen et al., Dynamic modeling and simulation of shell gasifier in IGCC. Fuel Process. Technol. **92**, 1418–1425 (2011). https://doi.org/10.1016/j.fuproc.2011.02.017
[8] F. Casella, P. Colonna, Dynamic modeling of IGCC power plants. Appl. Therm. Eng. **35**, 91-111 (2012). https://doi.org/10.1016/j.applthermaleng.2011.10.011
[9] S. Li, Researching and Simulation of the Load Dispatching Control Strategy on Gas-stream Combined Cycle. (North China Electric Power University, 2009.)
[10] J.L. Zhang, The full scale simulation of S109FA gas-steam combined cycle. (Southeast University, 2005.)
[11] X.T. Zhang, X.Q. Huang, Simulation of Biomass Gasification Coupled with Micro-Gas Turbine Power Generation System. Energy Research and Management **3**, 48-52 (2021). https://doi.org/10.16056/j.2096-7705.2021.03.010
[12] Y.N. Ren, J. Shen, J.L. Zhang, Modeling and Dynamic simulation of a blast furnace gas-steam combined cycle system. Journal of Chinese Society of Power Engineering **40**, 965-974 (2020). https://doi.org/10.19805/j.cnki.jcspe.2020.12.003
[13] L.P. Fan, K.L. Liu, Application research of molten salt energy storage technology in gas-steam combined cycle systems. Power Equip. **33**, 160-163 (2019). https://doi.org/10.3969/j.issn.1671-086X.2019.03.003
[14] W. Sun, Simulation modeling and characteristic research of distributed energy system.(Southeast University, 2016.)
[15] F.F. Zuo, W. Han, M.Y. Yao, Application status and development trend of molten salt energy storage in novel power systems. Thermal Power Generation **52**, 1-9 (2023). https://doi.org/10.19666/j.rlfd.202210230
[16] L.S. Zhong, Design and research on gas turbine speed control system. (Northeastern University, 2015.)
[17] X.C. Shen, Y. Fu, J.Y. Zhang, Study on the effect of thermal deformation on the liquid seal of high-temperature molten salt pump in molten salt reactor. Nucl. Sci. Tech. **34**, 27 (2023). https://doi.org/10.1007/s41365-023-01179-2
[18] S. Cennerilli, E. Sciubba, Application of the CAMEL process simulator to

the dynamic simulation of gas turbines. Energy Convers. Manag. **48**, 2792–2801 (2007). https://doi.org/10.1016/j.enconman.2007.06.048
[19] L.Y. Fang, D.F. Liu, X. He, Research on the precise step fitting method of compressorcharacteristic map. Gas Turbine Experiment and Research **32**, 21-27 (2019).
[20] A. Mehrpanahi, G. Payganeh, M. Arbabtafti, Dynamic modeling of an industrial gas turbine in loading and unloading conditions using a gray box method.Energy **120**, 1012-1024 (2017). https://doi.org/10.1016/j.energy.2016.12.012
[21] J.Y. Wu, J.L. Wang, S. Li et al., Experimental and simulative investigation of a micro-CCHP(micro combined cooling, heating and power) system with thermal management controller. Energy **68**, 444-453 (2014). https://doi.org/10.1016/j.energy.2014.02.057
[22] B.T. Aklilu, S.I. Gilani, Mathematical modeling and simulation of a cogeneration plant. Appl. Therm. Eng. **30**, 2545-2554 (2010). https://doi.org/10.1016/j.energy.2014.02.057
[23] S.S. Bishal, D. F. Faysal, M.M. Ehsan et al., Performance evaluation of an integrated cooling and power system combining supercritical CO_2, gas turbine, absorption refrigeration, and organic rankine cycles for waste energy recuperating system. Results Eng. **17**, 100943 (2023). https://doi.org/10.1016/j.rineng.2023.100943
[24] J. Chen, Modeling and Simulation of Gas and Steam Combined Cycle Based on a certain Gas Turbine.(Shanghai Jiao Tong University, 2010.)
[25] J. Xu, Simulation modeling and startup process optimization of HRSG in combined cycle plant. (Southeast University, 2017.)
[26] S.T. Guan, Calculation method research on main steam flow for turbine. Northeast. Electr. Power Technol. **38**, 47-48 (2017). https://doi.org/10.3969/j.issn.1004-7913.2017.02.015
[27] M.Y. Li. Modeling and control law research for gas turbine. (Institute of Engineering Thermophysics Chinese Academy of Science, 2016.)
[28] F. Xia, J.Q. Huang, W.X. Zhou, Modeling of and simulation research on turbofan engine based on Matlab / Simulink. Journal of Aerospace Power **22**, 2134-2138 (2007). https://doi.org/10.13224/j.cnki.jasp.2007.12.029
[29] Y. Lin, X.A. Pan, Z.S. He et al., Review of Peak Regulation for Power System With aHigh Penetration of Nuclear Power. Modern Electric Power **37**, 1 (2020). https://doi.org/10.19725/j.cnki.1007-2322.2019.0004
[30] Z.M. Zhu, Z. Jiang, B.B. Peng, Feasibility study of an ultra-high temperature molten salt energy storage demonstration project. SINAP-Q1044K-A-01. 2022 [internal report]